GKSS FORSCHUNGSZENTRUM in der HELMHOLTZ GEMEINSCHAFT

GPS Atmosphere Sounding Project – An Innovative Approach for the Recovery of Atmospheric Parameters

WP 232 – Validation of Regional Models – BALTEX – and Contributions to WP 341 and WP 344

Author:
K.-P. Johnsen

GKSS 2003/34

ISSN 0344-9629

HELMHOLTZ GEMEINSCHAFT GKSS ist Mitglied der Hermann von Helmholtz-Gemeinschaft Deutscher Forschungszentren e.V.

GKSS 2003/34

GPS Atmosphere Sounding Project – An Innovative Approach for the Recovery of Atmospheric Parameters

WP 232 – Validation of Regional Models – BALTEX – and Contributions to WP 341 and WP 344

Author:

K.-P. Johnsen

(Institute for Coastal Research)

GKSS-Forschungszentrum Geesthacht GmbH • Geesthacht • 2003

Die Berichte der GKSS werden kostenlos abgegeben.
The delivery of the GKSS reports is free of charge.

Anforderungen/Requests:

GKSS-Forschungszentrum Geesthacht GmbH
Bibliothek/Library
Postfach 11 60
D-21494 Geesthacht
Germany
Fax.: (49) 04152/871717

Als Manuskript vervielfältigt.
Für diesen Bericht behalten wir uns alle Rechte vor.

ISSN 0344-9629

GKSS-Forschungszentrum Geesthacht GmbH · Telefon (04152)87-0
Max-Planck-Straße · D-21502 Geesthacht / Postfach 11 60 · D-21494 Geesthacht

GKSS 2003/34

GPS Atmosphere Sounding Project – An Innovative Approach for the Recovery of Atmospheric Parameters

WP 232 – Validation of Regional Models – BALTEX – and Contributions to WP 341 and WP 344

Klaus-Peter Johnsen

37 pages with 14 figures and 6 tables

Abstract

The atmospheric water vapor content is one of the most important parameters for the hydrological cycle. In order to investigate the energy and water balance over the BALTEX study region this report describes comparisons of specific humidity profiles of the hydrostatic **H**igh resolution **R**egional weather forecast **M**odel HRM of the Deutscher Wetterdienst (DWD) with profiles derived from spaceborne radio occultation data of GPS/MET and CHAMP and comparisons with the vertically integrated water vapor (IWV) of different networks of groundbased GPS receivers within Europe.

High correlations (with a correlation coefficient around 0.9) between the HRM IWV and GPS IWV were found. It is shown that the analysis data used to initialize the HRM model can explain a large part of the mean difference between the IWV from the model and the GPS data.

Specific humidities and the IWVs were determined from the refractivity profiles of the radio occultations of GPS/MET and CHAMP/GPS using an iterative algorithm of Gorbunov and Sokolovski (1993). The comparisons of the specific humidity profiles have shown that both receivers, GPS/MET and CHAMP/GPS, measure significantly lower mean specific humidities below about 4 km than HRM. This is e.g. supported by comparisons between the HRM model and the ECMWF analysis data, between the HRM model and radiosonde ascents at Lindenberg/Germany (which have shown lower mean absolute differences of about 0.2 g/kg) as well as between HRM and further spaceborne data like AMSU-A/B and TERRA/MODIS.

Comparisons between CHAMP/GPS and AMSU-A over oceans and AMSU-B over Antarctica show the high value of GPS radio occultations for applications worldwide.

GPS-Atmosphären-Sondierung – Ein innovativer Ansatz zur Bestimmung atmosphärischer Parameter

Arbeitspaket 232 – Validation eines Regionalmodells – BALTEX – und Beiträge zu den Arbeitspaketen 341 und 344

Zusammenfassung

Der atmosphärische Wasserdampf ist einer der wichtigsten Parameter des Wasserkreislaufes. Im Rahmen der Untersuchung des Energie- und Wasserkreislaufes über dem BALTEX-Gebiet

beschreibt dieser Bericht Vergleiche von Vertikalprofilen der spezifischen Feuchte (IWV), die mit dem hydrostatischen und hochauflösenden Wettervorhersagemodell HRM (High Resolution Regional Model) des Deutschen Wetterdienstes bestimmt wurden, mit Profilen, die aus Radiookkultationsdaten von GPS und CHAMP abgeleitet wurden. Darüberhinaus werden Vergleiche des vertikal integrierten Wasserdampfes, bestimmt mit verschiedenen GPS Netzen über Europa, mit dem HRM-Modell verglichen.

Hohe Korrelationen (mit Korrelationskoeffizienten um 0,9) wurden zwischen HRM IWV und GPS IWV gefunden. Darüberhinaus wurde gezeigt, dass die Analysedaten, welche zur Initialisierung des HRM-Modells verwendet wurden, einen großen Teil der mittleren Differenz zwischen HRM IWV und GPS IWV erklären können.

Zur Bestimmung der Profile der spezifischen Feuchte aus Radiookkultationsdaten von GPS/MET und CHAMP diente ein iterativer Algorithmus von Gorbunov und Solkolovski (1993). Die Vergleiche der spezifischen Feuchteprofile mit HRM haben gezeigt, dass beide Empfänger, GPS/MET und CHAMP/GPS, signifikant niedrigere spezifische Feuchte unterhalb von 4 km Höhe bestimmen. Dieses wird unterstützt durch Vergleiche zwischen dem HRM-Modell und ECMWF-Analysedaten, zwischen HRM und Radiosondenaufstiegen in Lindenberg (Deutschland) sowie zwischen HRM und weiteren Satellitendaten wie AMSU-A/B und TERRA/MODIS. Radiosondendaten zeigten dabei niedrigere mittlere Differenzen zum HRM von etwa 0,2 g/kg.

Vergleiche zwischen CHAMP/GPS und AMSU-A über den Ozeanen sowie AMSU-B über der Antarktis zeigen den großen Wert der Radiookkultationsdaten für Anwendungen weltweit.

Manuscript received / Manuskripteingang in TDB: 20. November 2003

Contents

Chapter 1

Introduction

Water vapor is a key element in the climate of the Earth and in the hydrological cycle which describes the movement of water within and between the Earth's atmosphere, oceans, and continents. Water vapor is the most variable of the major components of the atmosphere (Bevis et al., 1992) and a critical element in short term numerical weather prediction (Kuo et al, 1993, 1996; Cucurell et al., 2000). Due to the transfer of energy via its phase changes it drives atmospheric circulations. It is also the dominant greenhouse gas (e.g. Jones and Mitchell, 1991; Read et al., 1995).

To observe the vertically integrated water vapor (IWV) within the atmosphere different groundbased and spaceborne remote sensors are available, e.g. radiosondes, Raman lidar, Global Positioning System receivers, AMSU receivers onboard the NOAA Polar Orbiting Satellites (e.g. Weng et al., 2000, Johnsen and Kidder, 2002; Johnsen et al., 2002), ERS-2/InSAR (e.g. Hanssen et al., 1999), the Special Sensor Microwave Imager (e.g. Schlüssel and Emery, 1990) or the Special Sensor Microwave Water Vapor Sounder (SSM/T2; Miao, 1998). While spaceborne remote sensors improve the spatial coverage compared with radiosondes the groundbased receivers allow a significant improvement of the temporal resolution. For a more complete review of the different systems and further details see Raschke (2002).

In order to investigate the water and energy balance over the BALTEX[1] region and its catchment this report describes

- comparisons of the vertically integrated water vapor as determined by networks of groundbased GPS receivers within Europe with the hydrostatic numerical weather prediction (NWP) model HRM (**H**igh resolution **R**egional **M**odel) of the Deutscher Wetterdienst (WP 232) and
- comparisons between the specific humidities derived from the HRM model, different spaceborne GPS radio occultations, radiosondes, and further spaceborne data (AMSU-A/B and TERRA/MODIS, WP 341/344).

Comparisons between CHAMP/GPS and AMSU-A over oceans and AMSU-B over Antarctica show the high value of GPS radio occultations for applications worldwide.

[1]The BALTic Sea EXperiment (BALTEX) is one of the continental scale experiments of the Global Energy and Water Cycle Experiment (GEWEX) build up by the World Meteorological Organization (WMO), the International Council of the Scientific Union (ICSU), and the Intergovernmental Oceanographic Commission, (IOC). For further details about BALTEX see e.g. Raschke et al. (2001) or http: //w3.gkss.de/baltex/baltex/.

Chapter 2

Groundbased and spaceborne GPS data

The US Global Positioning System (GPS) constellation currently consists of 29 satellites orbiting on six different planes inclined at 55°. Each satellite orbit is circular with a period of about 12 h and an altitude of 20200 km. It can be used to actively measure properties of the Earth's atmosphere and ionosphere by using groundbased or spaceborne receivers (Kursinski et al., 1997). The signals at both GPS frequencies (L_1 = 1.57542 GHz and L_2 = 1.22760 GHz) are delayed and refracted by the gases composing the atmosphere. Due to its permanent dipole moment, atmospheric water vapor introduces a significant and unique delay (for other components and their influence see *e.g.* Solheim et al., 1999).

The radio occultation technique has been applied for three decades to study planetary atmospheres of Mars (Fjeldbo and Eshleman, 1968), Venus (Fjeldbo and Kliore, 1971), Jupiter (Kliore et al., 1975; Hinson et al., 1997), Saturn (Lindal et al., 1985), Uranus (Lindal et al., 1987), and Neptune (Lindal, 1992).

Since the launch of the Low Earth Orbiter (LEO) Microlab-1 with the GPS/MET receiver onboard in April 1995 some satellites are carrying GPS receivers: The US-German satellite CHAMP (CHAllenging Microsatellite Payload) has obtained radio occultation profiles for around one year and about 215 profiles per day in 2002 (168 on average in 2001). Since the 10th of July 2001 radio occultation data from the US-Argentinian mission SAC-C are also available. Different missions with one or more GPS receivers are launched or planned, e.g. the US-German GRACE mission (e.g. http: //op.gfz−potsdam.de/grace/index_GRACE.html), or the US-Taiwanese COSMIC mission (e.g. http://www.cosmic.ucar.edu).

Limb sounding observations of the Earth's lower troposphere by a GPS receiver onboard a LEO allow to obtain sufficient accurate vertical profiles of temperature or water vapor. Future missions like the Earth Opportunity Mission ACE+ (Atmosphere and Climate Explorer Mission; Hoeg and Kirchengast, 2002) of ESA or the BRIGHTOC mission (Bi-static Radar Imaging of Geopotential, Humidity, Temperature, Ozone and Clouds, Kursinski et al., 2002) of NASA will use the LEO-LEO concept. By using phase and amplitude of several monochromatic signals near the 22 GHz water vapor line and (in case of BRIGHTOC) also at the 183 GHz water vapor line and the 195 GHz ozone line, these missions will allow to obtain absorption profiles as well as refractivity profiles. In contrast to the other missions mentioned these mission will allow to determine both quantities, water vapor and temperature, together.

To derive the water vapor from the radio occultation refractivity profiles an algorithm similar to that of Gorbunov and Sokolovskij (1993) was applied: This iterative algorithm starts with the assumption of a dry atmosphere and calculates the density using the ionosphere free refractivities N together with an interpolated temperature profile T taken from ECMWF or an numerical weather predition (NWP) model. The refractivities were derived by the GeoForschungsZentrum (GFZ, Potsdam) or the University Corporation for Atmospheric Research (Hajj et al., 2002) using the Abelian inversion. The hydrostatic equation is applied to obtain the pressure profile $P(z)$ using the constant of gravity g which is calculated according to

$$\begin{aligned} g &= (1 - 0.0026373\cos\phi - 5.9 \times 10^{-6}\cos^2\phi) \times \\ &\quad \times (1 - 3.14 \times 10^{-4} z) \times g_{45} \end{aligned} \tag{2.1}$$

from the height z and the latitude ϕ of the occultation. g_{45} is the constant of gravity at 45° latitude with $g_{45} = 9.80616\ \mathrm{m/s^2}$. The refractivity N is related to atmospheric parameters via

$$\begin{aligned} N(z) = \kappa_1 \frac{P(z)}{T(z)} + \kappa_2 \frac{P_w(z)}{T^2(z)} - 40.3 \times 10^6 \frac{n_e(z)}{f^2} + \\ O(\frac{1}{f^3}) + a_w W_w(z) + a_i W_i(z). \end{aligned} \tag{2.2}$$

P is the pressure, T the temperature, P_w is the water vapor pressure, n_e the electron density, f the operating frequency, W_w and W_i the liquid water and ice content, respectively. The last two terms are small compared to the others and will be neglected here. A ionospheric correction is applied according to Vorob'ev and Krasil'nikova (1994) and we restrict our considerations to the troposphere, thus the third and fourth term are also neglected. Here the constant κ_1 is equal to 77.6 K/hPa, κ_2 is $3.73 \times 10^5 \mathrm{K^2/hPa}$, a_w is $1.4 \times 10^3 \mathrm{m^3/kg}$ and a_i is $0.6 \times 10^3 \mathrm{m/kg}$. From equation (2.2) the water vapor pressure profile will be calculated and from

$$q(z) = \frac{0.622 \times P_w(z)}{P(z) - 0.378 \times P_w(z)} \tag{2.3}$$

the specific humidity profile $q(z)$. These equations were iterated to obtain profiles of $P(z)$, $P_w(z)$ and $q(z)$. Less than four iterations were necessary. Finally a cubic spline of $q(z)$ was integrated from the surface up to the uppermost layer to obtain the vertically IWV.

For comparisons of the vertically integrated water vapor the network of the GFZ mainly over Germany and the SWEPOS network over Sweden and Finland were applied. For further details see chapter 4.

Chapter 3

The High Resolution Regional Model HRM

The hydrostatic **H**igh resolution **R**egional **M**odel HRM of the Deutscher Wetterdienst (DWD) is compared with groundbased GPS, GPS radio occultation data, AMSU-A, TERRA/MODIS, radiosonde and ECMWF data. It is nearly the same as the regional forecast model Europamodell (EM) of the DWD (Majewski, 1991).

Table 3.1: Parameter calculated with the HRM model. [1]: Dimension in latitude, longitude and height. See also next table.

Element	Description	Unit	Dimension[1]
AK	AK – Hybrid level parameter	1	31, 0, 0
BK	BK – Hybrid level parameter	1	31, 0, 0
FIS	Orography × g	m^2/s^2	241, 241, 0
Z0	Roughness length total	m	241, 241, 0
FR_{LAND}	Land fraction of surface	1	241, 241, 0
SOILTYP	Soil type	1	241, 241, 0
PLCOV	Plant cover	%	241, 241, 0
ROOT	Root depth	m	241, 241, 0
U	U-velocity	m/s	241, 241, 30
V	V-velocity	m/s	241, 241, 30
T	Temperature	K	241, 241, 30
QV	Specific humidity	kg/kg	241, 241, 30
QC	Cloud water	kg/kg	241, 241, 30
PS	Surface pressure	Pa	241, 241, 0
T_{SNOW}	Temperature at top of snow	K	241, 241, 0
T_G	Surface temperature	K	241, 241, 0
T_S	Temperature at bottom of snow	K	241, 241, 0
T_M	Temperature at bottom of 1. soil layer	K	241, 241, 0
T_{CL}	Climat. temperature at bottom of the soil	K	241, 241, 0
W_{SNOW}	Water content of snow	mmH_2O	241, 241, 0
W_I	Water content of interception storage	mmH_2O	241, 241, 0
W_{G1}	Water content of 1. soil layer	mmH_2O	241, 241, 0
W_{G2}	Water content of 2. soil layer	mmH_2O	241, 241, 0

Table 3.2: Parameter calculated with the HRM model (cont.).[1]: Dimension in latitude, longitude and height. TOA: top of atmosphere; BOA: bottom of atmosphere.

Element	Description	Unit	Dimension[1]
QV_S	Specific humidity at the surface	kg/kg	241, 241, 0
T_{2M}	2 metre temperature	K	241, 241, 0
TD_{2M}	2 metre dew point temperature	K	241, 241, 0
U_{10M}	10 metre U-velocity	m/s	241, 241, 0
V_{10M}	10 metre V-velocity	m/s	241, 241, 0
TKVM	Diffusion coefficient of momentum	m^2/s	241, 241, 30
TKVH	Diffusion coefficient of heat	m^2/s	241, 241, 30
$SOHR_{RAD}$	Solar radiation heating rate	K/s	241, 241, 30
$THHR_{RAD}$	Thermal radiation heating rate	K/s	241, 241, 30
CLC	Cloud Cover	%	241, 241, 30
ALB_{RAD}	Shortwave albedo at the surface	1	241, 241, 0
$SOBS_{RAD}$	Solar radiation balance at the surface	W/m^2	241, 241, 0
$THBS_{RAD}$	Thermal radiation balance at the surface	W/m^2	241, 241, 0
$SOBT_{RAD}$	Solar radiation balance at TOA	W/m^2	241, 241, 0
$THBT_{RAD}$	Thermal radiation balance at TOA	W/m^2	241, 241, 0
CLCH	High cloud cover	%	241, 241, 0
CLCM	Medium cloud cover	%	241, 241, 0
CLCL	Low cloud cover	%	241, 241, 0
CLCT	Total cloud cover	%	241, 241, 0
$ASOB_S$	Average solar rad. balance at BOA	W/m^2	241, 241, 0
$ATHB_S$	Average thermal rad. balance at BOA	W/m^2	241, 241, 0
$APAB_S$	Average photosynt. act. rad. bal. at BOA	W/m^2	241, 241, 0
$ASOB_T$	Average solar radiation balance at TOA	W/m^2	241, 241, 0

It allows to derive as prognostic variables the surface pressure, the temperature, water vapor, cloud water, and the horizontal wind components. It is based on a rotated spherical Arakawa C-grid with hybrid vertical coordinates and is derived from a geographic system which is rotated by Eulerian angles such that the North pole is moved to a new position. For all calculations shown within this report the latitude of the North Pole was 32.5° N and the longitude 170.0° W. A mass flux convection scheme after Tiedtke (1976) and a delta-two-stream radiation scheme after Ritter and Geleyn (1992) for short- and longwave fluxes enabling the full cloud-radiation feedback mechanism are included. A two-layer soil model after Jacobsen and Heise (1982) including the snow and the interception storage is also included. The lateral boundaries are handled numerically such that large-scale meteorological systems can be taken from the driving model with as little damping as possible. Small-scale systems and gravity waves are able to leave the model domain without to much reflection at the lateral boundaries. The HRM uses the method of Davies (1976). This method has proved to be successful in a number of operational regional models.

The HRM used as boundary conditions interpolated 6-hourly EM3AN analyses of the Europa-Modell of the DWD or 6-hourly analyses of the ECMWF (European Centre for Medium-Range Weather Forecast). Three different runs were performed:

Table 3.3: Parameter calculated with the HRM model (cont.).[1]: Dimension in latitude, longitude and height. TOA: top of atmosphere; BOA: bottom of atmosphere.

Element	Description	Unit	Dimension[1]
$ATHB_T$	Average thermal radiation balance at TOA	W/m^2	241, 241, 0
CLC_{CON}	Convective cloud cover	%	241, 241, 30
DT_{CON}	Temperature tendency due to convection	K/s	241, 241, 30
DQV_{CON}	Spec. humidity tendency due to convect.	kg/(kg × s)	241, 241, 30
DU_{CON}	Zonal wind tendency due to convection	m/s^2	241, 241, 30
DV_{CON}	Meridional wind tendency due to convect.	m/s^2	241, 241, 30
PRR_{CON}	Precipitation rate, rain, convective	$kg/(m^2 \times s)$	241, 241, 0
PRS_{CON}	Precipitation rate, snow, convective	$kg/(m^2 \times s)$	241, 241, 0
BAS_{CON}	Base index of main convective cloud	1	241, 241, 0
TOP_{CON}	Top index of main convective cloud	1	241, 241, 0
$HBAS_{CON}$	Base height of main convective cloud	m	241, 241, 0
$HTOP_{CON}$	Top height of main convective cloud	m	241, 241, 0
$HTOP_{DC}$	Top height of dry convection	m	241, 241, 0
DQC_{GSP}	Cloud water tend of grid scale precip	kg/(kg×s)	241, 241, 30
QRS_{GSP}	Precip. particles for water load.	kg/kg	241, 241, 30
PRR_{GSP}	Precipitation rate, rain, grid scale	$kg/(m^2 \times s)$	241, 241, 0
PRS_{GSP}	Precipitation rate, snow, grid scale	$kg/(m^2 \times s)$	241, 241, 0
$RAIN_{GSP}$	Precipitation amount, rain, grid scale	kg/m^2	241, 241, 0
$SNOW_{GSP}$	Precipitation amount, snow, grid scale	kg/m^2	241, 241, 0
$RAIN_{CON}$	Precipitation amount, rain, convective	kg/m^2	241, 241, 0
$SNOW_{CON}$	Precipitation amount, snow, convectiv	kg/m^2	241, 241, 0
$RUNOFF_S$	Surface water run-off	kg/m^2	241, 241, 0
$RUNOFF_G$	Ground water run-off	kg/m^2	241, 241, 0
$AUMFL_S$	Average u-momentum flux at the surface	$kg/(m \times s^2)$	241, 241, 0
$AVMFL_S$	Average v-momentum flux at the surface	$kg/(m \times s^2)$	241, 241, 0
$ASHFL_S$	Average sensible heat flux at the surfac	W/m^2	241, 241, 0
$ALHFL_S$	Average latent heat flux at the surface	W/m^2	241, 241, 0

For the **PIDCAP** period (**P**ilot Study for **I**ntensive **D**ata **C**ollection and **A**nalysis of **P**recipitation; August 1 to November 17, 1995) two runs with different analysis data (EM3AN and ECMWF) were calculated and for the **BALTEX/BRIDGE** period (between 1st of October 1999 and 28th of February 2002) the ECMWF analysis data were applied. The model was initialized by interpolation of the 0 h analysis. It calculated the water vapor with a horizontal resolution of 0.125° (about 14×14 km^2) in 30 vertical layers up to about 25 km height and the other parameters as shown in tables 3.1 to 3.3. The vertical coordinate η of the model defines a so called hybrid system where $\eta = \eta(p, p_s)$ is a monotonic function of the pressure p and depends also on the surface pressure p_s. The time step was chosen to 90 s. Consecutive 30 h forecasts starting each day at 0 UTC including a 6 h spin-up time of the model were performed.

Chapter 4

Groundbased GPS data

4.1 Comparisons with NWP model data of the PIDCAP period

The quality of the technique to estimate the IWV from groundbased GPS measurements has been considered in many studies with up to 25 GPS receivers (e.g. Rocken et al., 1993, 1995; Emardson et al., 1998). Here we are using a dataset of the EU funded project NEWBALTIC (Numerical Studies of the Energy and Water Cycle of the Baltic Region) obtained from 20 continuously operating GPS stations in Sweden (SWEPOS network) and 5 sites in Finland, belonging to the Finnish permanent GPS network (Figure 4.1). The data were obtained from the Onsala Space Observatory, Onsala, Sweden, and the Finnish Geodetic Institute. Details about the measurement procedure were described e.g. by Emardson et al., 1998.

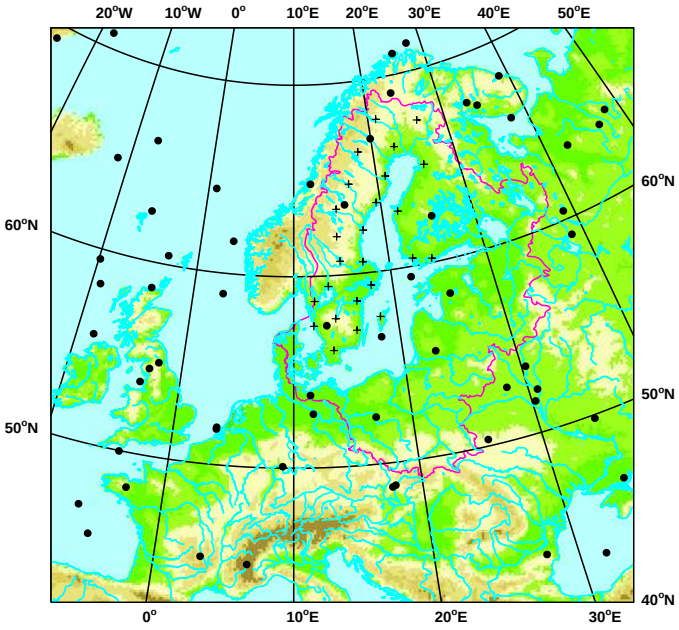

Figure 4.1: BALTEX area with NEWBALTIC stations (plus symbols) and GPS/MET radio occultations (points) during PIDCAP.

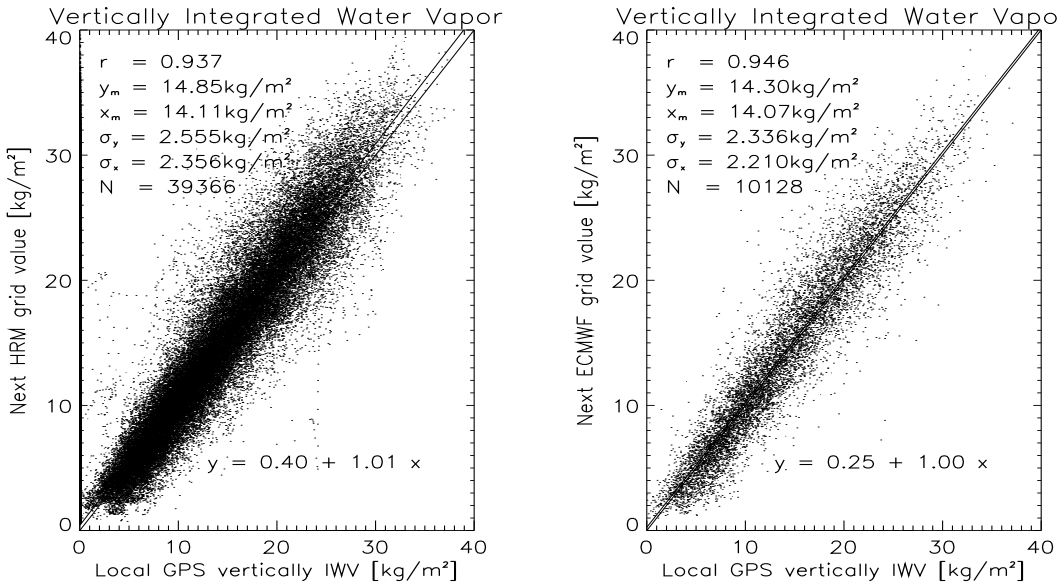

Figure 4.2: **Left:** Comparison of the vertically IWV derived from HRM and from the NEWBALTIC groundbased network. r is the correlation coefficient between both datasets and x_m and y_m are the mean values of the GPS IWV and HRM IWVs, respectively. σ_x and σ_y are the standard deviations between the least square fit and the GPS IWV or HRM IWV, respectively, and N is the number of measurements. **Right:** Comparison of the vertically IWV derived from 6-hourly ECMWF-analyses as initial fields for HRM and from the NEWBALTIC groundbased network within the PIDCAP period. For explaination of r,y_m,x_m,σ_x,σ_y and N see left Figure.

The GPS data were obtained every 5 min., while hourly derived forecasts with the HRM model were compared with one hour mean values of the GPS network. Thus altogether 39366 matches were obtained within these roughly 3.5 months of the observation period. Figure 4.2 (left) shows the comparison of the vertically IWV derived from HRM and from the NEWBALTIC groundbased network. The HRM model overestimates slightly the IWV as derived from GPS data (≈ 0.74 kg/m^2). The standard deviation $\sigma_{HRM} = 2.555$ kg/m^2 is about 6 % of the total range of IWV measurements. A linear regression between the GPS data (G) and the HRM model (H) gives $H = 0.40 + 1.01 \times G$.

Table 4.1 shows the differences between the IWV as derived from the HRM model and from the GPS data. The columns show the differences when different analysis data are used to initialize the HRM forecast model. EM3AN and ECMWF analysis show larger IWV compared to the GPS data. The differences are larger by using the EM3AN analysis data of the Europa model of the DWD in comparison with use of ECMWF analysis data (Figure 4.2 right). The standard deviations are also slightly larger. The table shows that the mean differences can mainly be explained by the different analysis data, e.g. the HRM IWV as well as the IWV of the analysis data show higher mean values than the GPS IWV data. Especially the mean difference between the EM3AN analysis data as initial fields in the HRM model and the HRM IWV is very low (0.08 kg/m^2). The correlation coefficients between GPS data and the model data are large (larger than 0.92).

Table 4.1: *CC* means correlation coefficient and $HRM - GPS$ ($Analysis - GPS$) the mean differences between the IWV of the HRM (IWV of the analysis data) and the GPS data. The columns show the different results obtained with ECMWF analysis data or with EM3AN analysis data as initial fields for the HRM model. σ_{HRM} and $\sigma_{Analysis}$ are the standard deviations of the IWV of the HRM model and the analysis compared with the **NEWBALTIC** GPS data, respectively.

	ECMWF-Analyses	EM3AN-Analyses
CC HRM	0.937	0.935
CC Analysis	0.946	0.925
HRM-GPS	0.74 kg/m^2	2.69 kg/m^2
Analyses-GPS	0.23 kg/m^2	2.77 kg/m^2
σ_{HRM}	2.555 kg/m^2	2.756 kg/m^2
$\sigma_{Analysis}$	2.336 kg/m^2	2.841 kg/m^2

4.2 Comparisons with NWP model data of the BRIDGE period

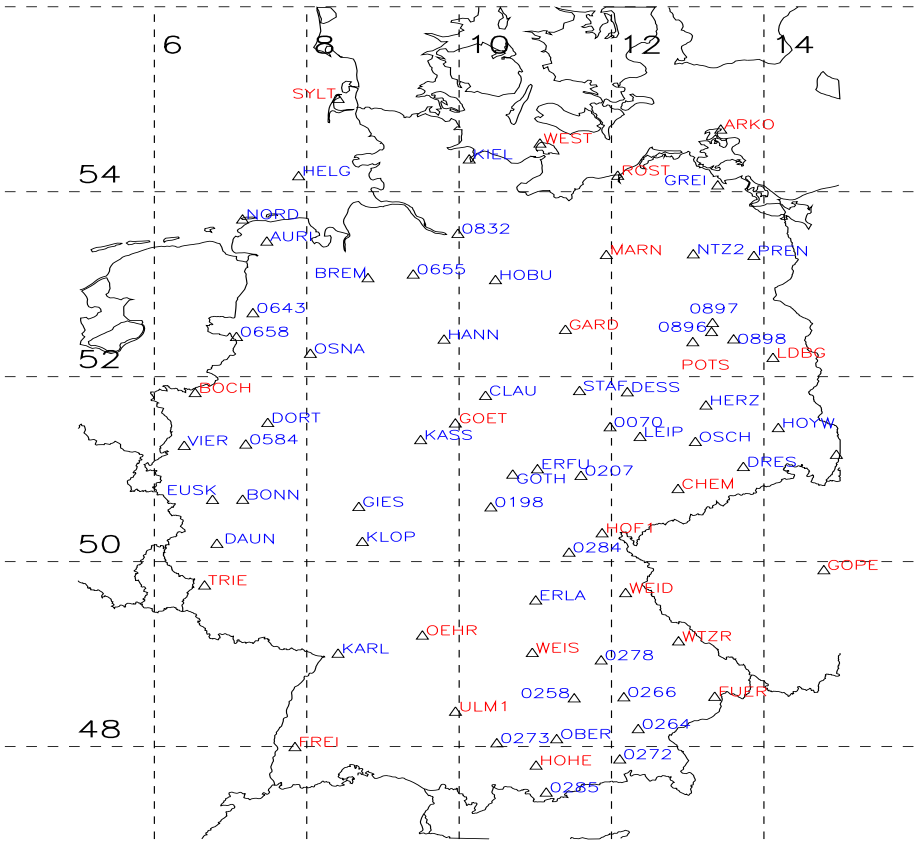

Figure 4.3: 74 GFZ/GPS stations mainly within Germany used within this study. Blue colored station names show stations equipped without pressure sensors while red colored station names show stations with pressure sensor.

Table 4.2: Mean differences and standard deviations between the IWV determined with the HRM model (HRM), from the GPS data (GPS) and from the ECMWF analysis data (ANA) used as boundary data for the initialisation of the HRM model. P: surface pressure, int: interpolated, obs: observed. [1] : RMS^2 = Mean difference^2+Standard deviation^2.

P	Meas. No.	HRM-ANA [kg/m^2]	RMS[1] [kg/m^2]	ANA-GPS [kg/m^2]	RMS[1] [kg/m^2]
int.	27700	0.03 ± 2.31	2.31	-0.18 ± 2.09	2.10
obs.	25071	-0.01 ± 2.30	2.30	0.40 ± 1.81	1.85
all	52771	0.01 ± 2.31	2.31	0.10 ± 1.99	1.99
P	Meas. No.	HRM-GPS [kg/m^2]	RMS[1] [kg/m^2]	Station No.	
int.	219916	-0.20 ± 2.58	2.58	50	
obs.	205547	0.36 ± 2.29	2.32	24	
all	425463	0.08 ± 2.47	2.47	74	

Here the GPS constellation together with a dense network of groundbased receivers is used to get a high spatial and temporal resolution of the vertically integrated water vapor over Germany (Figure 4.3). The GPS network consists of stations of the SAPOS network (SAtelliten POSitionierdienst) of the German Land Surveying Agencies and stations from the GeoForschungsZentrum (GFZ) build up at the weather stations of the DWD. Details about the processing of the GPS data are given by Gendt et al. (2001). During the first complete year with GFZ/GPS data within the BALTEX/BRIDGE baseline period (May 2000 to April 2001) altogether 74 stations of the GFZ/GPS network were available. For 24 stations (mainly at the DWD stations) pressure observations could be applied to derive the hydrostatic delay. For the other 50 stations the pressure values were interpolated from the dense synoptic network of the DWD. Statistics from this procedure reveal an error of

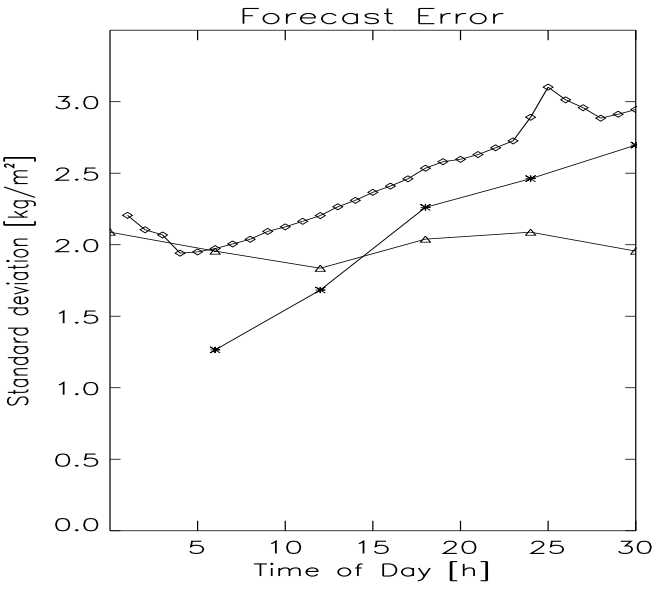

Figure 4.4: Standard deviation of the IWV differences HRM-GPS (rhombs), HRM-Analysis (asterisks) and Analysis-GPS (triangles) as function of the forecast time.

0.3 hPa rms (Gendt et al., 2001) corresponding to an IWV error of about 0.12 kg/m^2. This dataset is compared with the hydrostatic numerical weather prediction model HRM of the DWD.

The HRM/IWV as well as the GPS/IWV ranges are between 0 and 49 kg/m^2 within the observation period. Table 4.2 shows the mean differences and standard deviations between the IWV derived from the HRM model forecast after a 6 h period used as spin up time of the model, from the GPS data and from the ECMWF analysis data. Altogether 425463 matches between HRM/IWV and the GPS/IWV data and 52771 between the analysis data and the HRM or GPS data were obtained. The HRM model overestimates slightly the water vapor as observed with the GPS receivers. This mean difference can mainly be explained by the difference between the ECMWF analysis data and the GPS data.

The standard deviation at the stations with pressure sensors is about 0.29 kg/m^2 lower than at the stations without pressure sensors. Because the water vapor varies more in the lower atmosphere than in the upper atmosphere more model layers are included in the lower atmosphere. Thus the error introduced by interpolation of the specific humidity to derive the IWV is reduced. Nevertheless, this error together with the interpolation error of the network of the DWD (see above, Gendt et al., 2001) may explain a large part the rms difference. A small contribution is also introduced through the GPS receiver height level correction with the help of the hydrostatic equation. The IWV standard deviation of all stations increases with the forecast time. During the 6 h spin up time of the model the standard deviation decreases slightly. This is mainly due to the HRM model, the analysis data do not show an increase compared with the GPS data (Figure 4.4).

4.3 Comparison between HRM and AMSU-A data

The Advanced Microwave Sounding Unit A (AMSU A) onboard NOAA-15 and 16 allows retrieval of the IWV from passive microwave measurements. To derive the IWV the NOAA/NESDIS Total Precipitable Water (TPW) algorithm is used. It is described in Weng and Grody (2000) and is available on-line at http://orbit-net.nesdis.noaa.gov/arad2/MSPPS/html/day2/algorithm_day2.html. Two AMSU-channels are used: 23.8 GHz and 31.4 GHz. In brief the algorithm works because 23.8 GHz is near a water vapor rotation line and is more sensitive to water vapor absorption than to cloud water droplet absorption, whereas 31.4 GHz is in a window region and is more sensitive to cloud droplet absorption than to water vapor absorption. The different characteristics at the two frequencies are exploited to simultaneously retrieve IWV and vertically integrated cloud liquid water under both clear and cloudy conditions. Based on radiative transfer simulations Grody et al. (1999) have shown that the rms error of the AMSU-A/IWV is about 1 kg/m^2. Both frequencies are measured by the AMSU-A instrument, which has 48 km resolution at nadir. The IWV product is available at least four times per day, except near the equator, where there are gaps between satellite swaths.

To compare the HRM model results above the sea the Advanced Microwave Sounding Unit (AMSU) A is applied within the BALTEX area. Figure 4.5 shows 15356 IWV comparisons from colocated pixels of the AMSU-A and the HRM model for the AMSU passive microwave receiver onboard NOAA-15 between 26th and 30th of April 2001 (the AMSU-A data are available from the 26th of April 2001

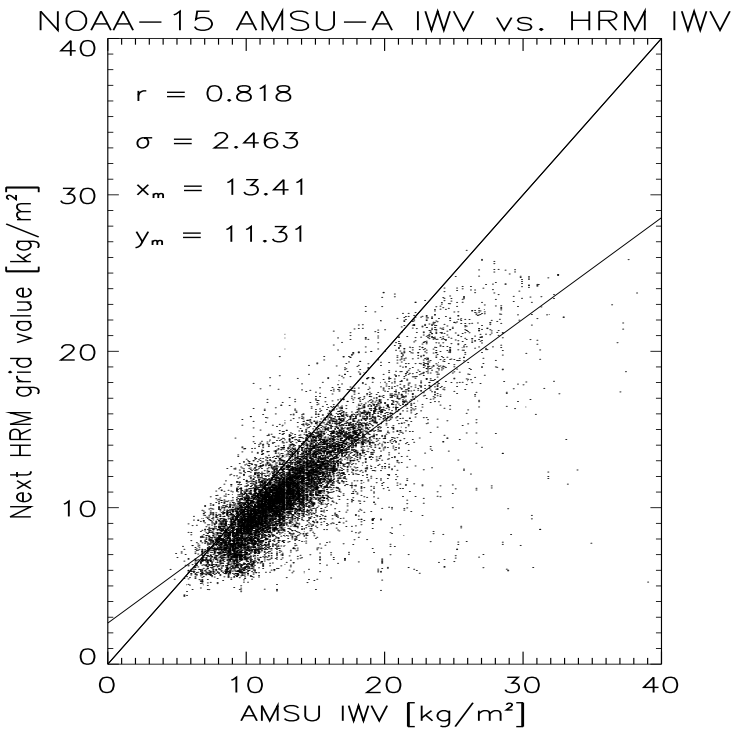

Figure 4.5: Integrated water vapor (IWV) derived from AMSU-A data of NOAA 15 between 26th and 30th of April 2001 over the sea within the BALTEX area compared with the IWV of the HRM model. r is the correlation coefficient, σ the standard deviation of the difference (HRM-AMSU), x_m the mean value of the AMSU IMV, y_m the mean value of the HRM IWV. The 1:1 line as well as a linear fit are given.

to present). To avoid spillover effects near land areas an adequate land mask is applied. The HRM shows slightly lower mean values compared with the AMSU-A data (Table 4.3). While the number of matched pixels is comparably large, like

Table 4.3: Δ is the mean difference between HRM/IWV and AMSU-A/IWV, r is correlation coefficient and N is the number of data compared.

	Δ	r	N
NOAA-15	-2.1 ± 2.5 kg/m^2	0.82	15356
NOAA-16	-2.2 ± 2.3 kg/m^2	0.84	14353

that between the GPS data and the HRM model above land, the standard deviation between both datasets (NOAA-15 ≈ 2.46 kg/m^2, NOAA-16 ≈ 2.29 kg/m^2), as well as the range of IWV values, are also similar. The underestimation of the AMSU-A IWV data increases with increasing water vapor within the atmosphere (see linear fit in Figure 4.5). The correlation coefficients of both datasets are with about 0.82 (NOAA-15) and 0.84 (NOAA-16) smaller than the correlation coefficient between the GPS data and the HRM model which is about 0.93.

Chapter 5

GPS radio occultation data

5.1 Comparison between HRM and ECMWF or radiosonde data

Figure 5.1 (left) shows mean specific humidity differences and their standard deviations of HRM and the ECMWF data between 14th of May and 10th of June 2001. 123 profiles of HRM and ECMWF colocated with the CHAMP/GPS data and interpolated to the GPS levels and times were used. The standard deviations are below 1 g/kg. The HRM model shows slightly (around 0.1 g/kg) smaller specific humidities for most of the heights below about 3 km and slightly larger specific humidities above 3 km. Similar results were obtained by comparing the HRM model results with 145 radiosonde ascents from Lindenberg/Germany between the 1st of May and the 6th of June 2000 (Figure 5.1, right). The standard deviations are below

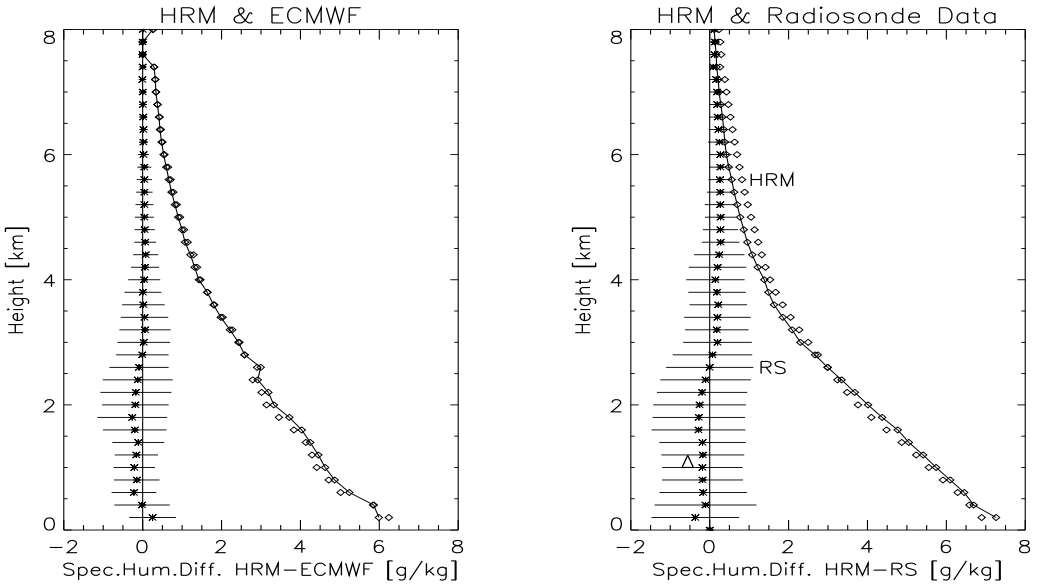

Figure 5.1: **Left:** Mean specific humidity differences between HRM (diamonds) and ECMWF data (diamonds with line) and their standard deviations. **Right:** Mean differences and standard deviations of the specific humidities derived from the HRM model (diamonds) and from 145 radiosonde profiles in Lindenberg/Germany (diamonds with line) between the 1st of May 2000 and the 6th of June 2000.

1.5 g/kg. The mean absolute differences are below 0.4 g/kg.

5.2 Comparison between GPS/MET and the HRM model

To compare the vertical water vapor profiles of the HRM with GPS/MET we interpolated the specific humidity as derived by HRM to the 200 m resolution of the 60 available GPS/MET data profiles: GPS/MET data of Prime Time 3 (October 12 to 27, 1995) with Anti-Spoofing (A/S) of the GPS L2 signal (i.e., the intentional encryption of the code modulation on L2) off were chosen because they were obtained within the PIDCAP period. The four spatially and temporally closest HRM grid points were used to compare with one radio occultation. The water vapor profiles of the GPS/MET were calculated using an algorithm similar to that of Gorbunov and Sokolovskiy (1993). The algorithm is described in chapter 2.

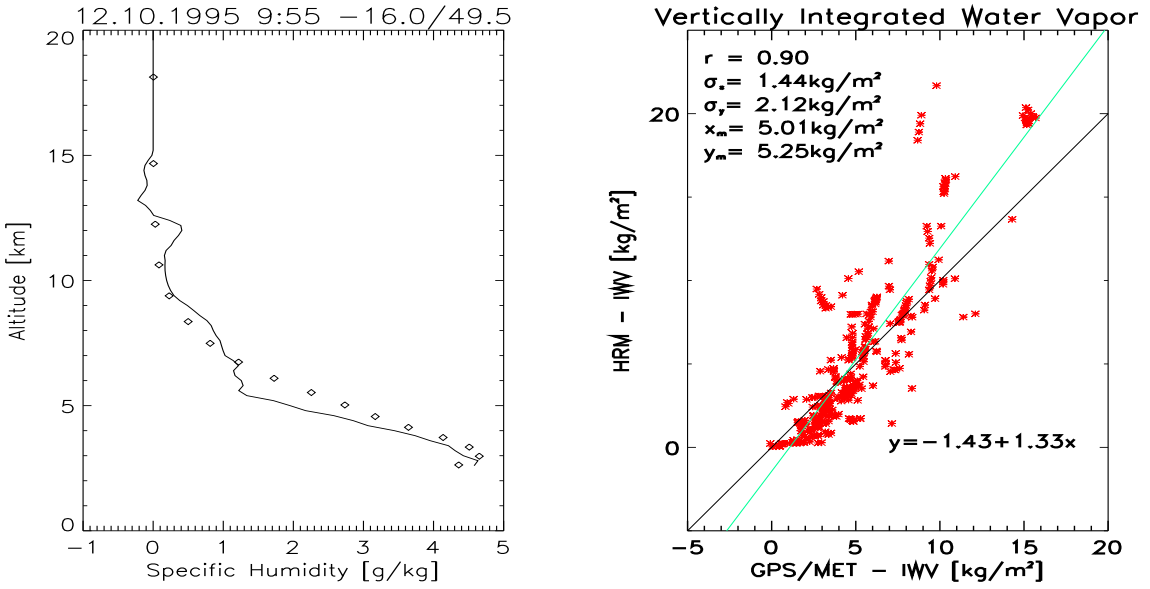

Figure 5.2: **Left:** Comparison of the water vapor within the troposphere as derived from GPS/MET (solid line) and with HRM (diamonds) at the 12th of October 1995. **Right:** Comparison of the IWV from GPS/MET and the IWV derived with HRM.

To get an overview over all profiles the vertically IWV of GPS/MET is compared with that of the HRM (Figure 5.2 right). Since the radio occultation measurements never reached the surface of the Earth the IWV was calculated from the lowest point of GPS/MET up to the tropopause as obtained from the HRM. The correlation between both datasets is quite large (correlation coefficient 0.90) but the GPS/MET shows significant lower values of the IWV than the HRM. The standard deviations are low ($\sigma_{HRM} = 1.44$ kg/m^2 and $\sigma_{GPS/MET} = 2.12$ kg/m^2). Figure 5.3 shows mean specific humidities as derived from GPS/MET and from HRM. The HRM model gives values which are about 20 % greater within the lower troposphere. Below about 2.2 km the specific humidities derived from GPS/MET decrease strongly due to e.g. multipath effects (Gorbunov and Gurvich, 1998) but less than 20 % of the radio occultations reach this low depth.

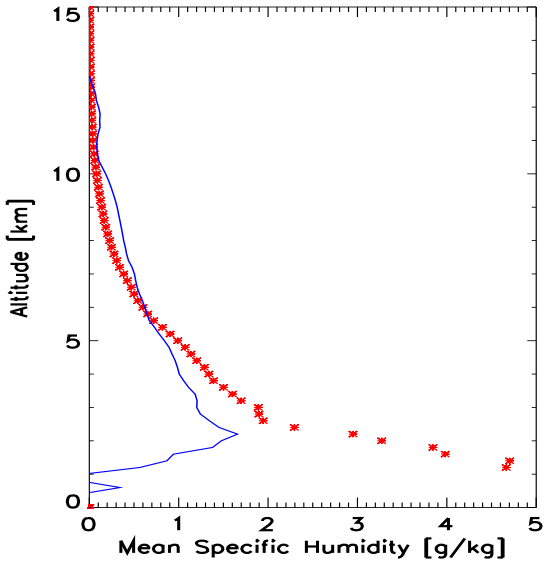

Figure 5.3: Mean specific humidities during PIDCAP as obtained from GPS/MET and from HRM (asterisks).

5.3 CHAMP/GPS and the HRM model

Figure 5.4 shows the mean tangent point positions for a dataset of 415 radio occultations of CHAMP/GPS over the BALTEX study region taken between the 14th of

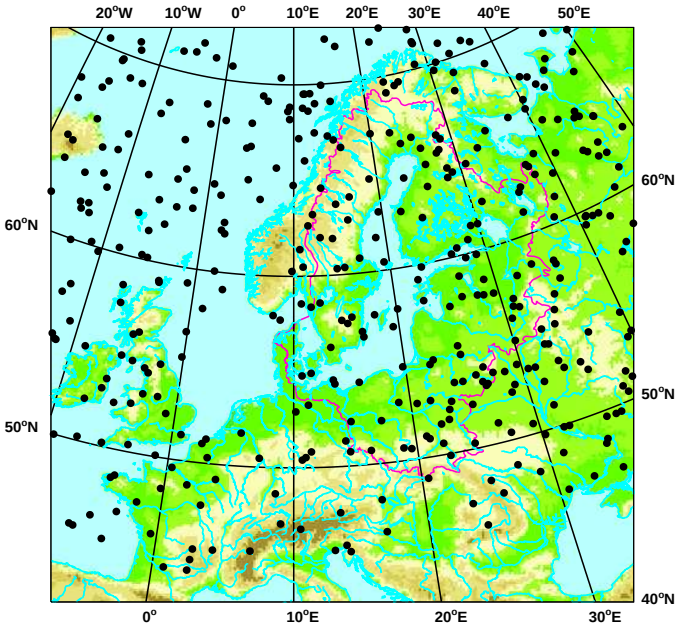

Figure 5.4: BALTEX area with mean CHAMP tangent point positions for the dataset of 415 radio occultations between the 14th of May 2001 and the 20th of January 2002.

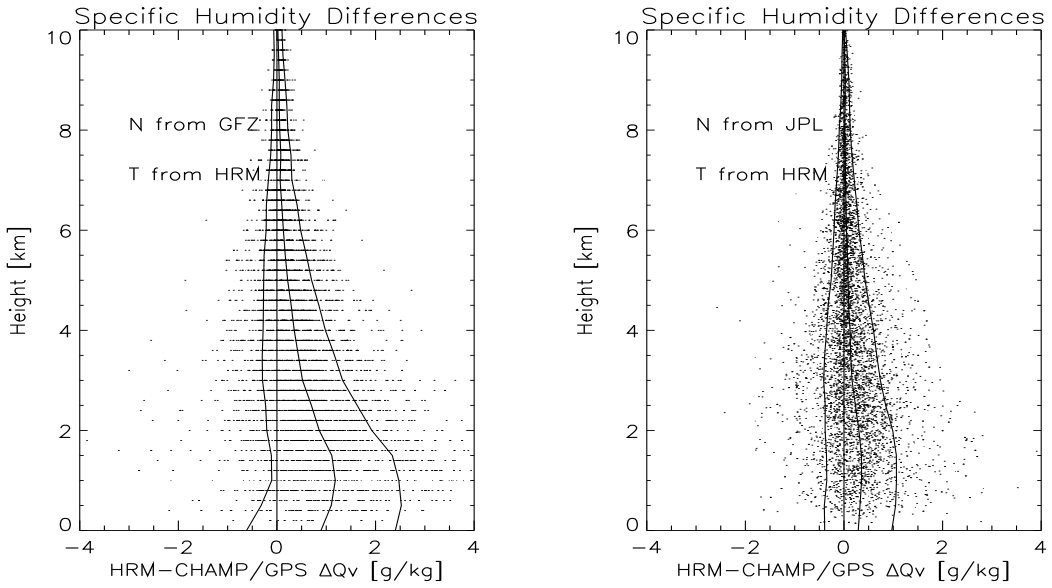

Figure 5.5: **Left:** Specific humidity differences between CHAMP/GPS and the HRM model using the refractivities derived by the GFZ, **right:** same as left, but using the refractivities derived by JPL.

May 2001 and the 20th of January 2002 during the BRIDGE period. Figure 5.5 left shows the specific humidity difference between CHAMP/GPS and the HRM model using the refractivities derived by the GFZ (Wickert, 2002). To derive the specific humidities the algorithm of Gorbunov and Sokolovskij (1993) is applied. The temperature profiles used are interpolated profiles of the HRM model. Figure 5.5 shows the same dataset but with refractivities derived by the Jet Propulsion Laboratory (JPL), Pasadena, CA, USA (Hajj et al., 2002). In both cases CHAMP/GPS shows lower mean specific humidities. The difference increases with decreasing height, maybe due to multipath effects within the lower troposphere (Gorbunov and Gurvich, 1998). However, recent studies show (Beyerle et al., 2002) that the bias problem of the CHAMP refractivities does not seem to be caused solely by multipath effects but corrections e.g. by the canonical transform method show an improvement of the data quality. Effects influencing the GPS phase tracking process causing cycle slips could maybe also explain the bias (Hajj et al., 2002).

5.4 Comparison between HRM and TERRA/MODIS

MODIS is a scanning spectroradiometer onboard the TERRA spacecraft with 36 spectral bands between 0.645 and 14.235 μm (Menzel et al., 1998). Following the approach of Smith et al. (1985) clear sky temperature and moisture profiles (MOD-07 product) together with the surface temperatures were calculated simultaneously with the help of a radiative transfer equation. Cloud filtering is achieved with the aid of the cloud mask product (MOD-06). The horizontal spatial resolution of one vertical profile is 5×5 km^2.
18142 vertically interpolated specific humidity profiles of TERRA/MODIS were compared with colocated profiles derived with the HRM model. The comparison for this dataset of the 1st of December 2001, 1100 UTC is shown in Figure 5.6:

Similar like the CHAMP/GPS dataset this dataset contains a large range of specific humidities (e.g. between 0.5 and 7.5 g/kg in a height of 1 km). It covers nearly the half of the BALTEX modelling area (MODIS data between 36.7° and 58.4° N and between −14.7° and 22.7° E). The HRM model shows slightly (around 0.5 g/kg) larger mean specific humidities for most of the heights between the surface and about 4 km. The standard deviation at the surface between both datasets ($\approx$ 2 g/kg) is a little bit larger compared with CHAMP/GPS. It decreases to less than 0.01 g/kg at 4 km height.

5.5 CHAMP/GPS and NOAA/AMSU-A/B

The lack of traditional meteorological observations over Antarctica and other remote areas like the South Pacific Ocean is a major challenge for the operational weather prediction as well as for the application of satellite data.

Here comparisons are shown between the vertically IWV derived from CHAMP / GPS data and from data of the Advanced Microwave Sounding Unit NOAA-15 / AMSU-B over Antarctica as well as from data of NOAA-15/AMSU-A over oceans.

Altogether 1932 profiles of CHAMP/GPS were obtained between the 14th of May 2001 and the 31th of May 2002 over Antarctica and vertically IWVs were calculated. Figure 5.7 shows running 60-day mean values of these vertically IWVs. It can be seen that the water vapor has a clear annual oscillation and is significantly larger in the austral summer compared to the austral winter. This is certainly related to the high air temperatures in summer. The annual mean value of the vertically CHAMP/GPS IWVs over Antarctica (between day 134 of 2001 and day 134 of year 2002) is about 1.56 ± 1.57 kg/m^2. With an area of the Antarctic continent of about 11.9×10^6 km^2 the annual mean of the total amount of atmospheric water vapor

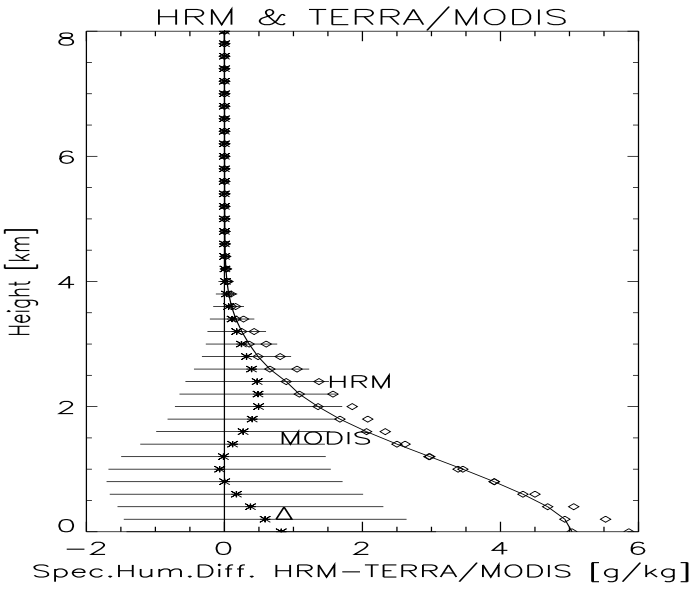

Figure 5.6: Mean specific humidities from HRM (diamonds) and TERRA/MODIS (diamonds with line) and its differences and standard deviations for 18142 pixels of the TERRA/MODIS dataset of 1st of December 2001, 1100 UTC.

over the entire continent is estimated to be about 1.9×10^{13}kg. Jacobs et al. (1992) obtained for the total accumulation through snow falling over the Antarctic ice sheet about 2.0×10^{15} kg/yr. This shows, that the mean residence time of water vapor over Antarctica is only 3 to 4 days, which is significantly shorter than the global mean of 9 to 10 days (Howarth, 1983). Similar results were obtained by Miao et al. (2001) from data of the spaceborne microwave water vapor sounder SSM/T2 onboard DMSP spacecraft F12 and F14 for the year of 1997.

The Advanced Microwave Sounding Unit-B onboard the NOAA Polar Operational Environmental Satellite NOAA-15 is a cross-track, line scanning instrument designed to measure scene radiances in the 5 channels at 89.0 ± 0.9, 150.0 ± 0.9, 183.31 ± 1.0, 183.31 ± 3.0 and 183.31 ± 7.0 GHz. Ninety contiguous scene resolution cells are sampled in a continuous fashion, each scan covering 50 degrees on each side of the subsatellite path. These scan patterns and geometric resolution translate to a 16.3 km diameter cell at nadir at a nominal altitude of 850 km.

To derive the vertically IWV from AMSU-B data an algorithm of Miao et al. (2001) is used. The algorithm was originally developed for the water vapor sounder DMSP-SSM/T2 but due to the same frequencies available from AMSU-B it can also be applied to AMSU-B data. It uses the four highest frequencies at 150.0 and 183.31 GHz (channels 17 to 20). A general form of the radiative transfer equation of Guissard and Sobieski (1994) is applied taking into account the effects of diffuse scattering from the ground surface and of the vertical nonuniformity of the atmosphere. In brief the algorithm calculates the water vapor, defining a new quantity

$$\eta_c = \frac{\Delta T_{ij} - b_{ij}}{\Delta T_{jk} - b_{jk}}, \tag{5.1}$$

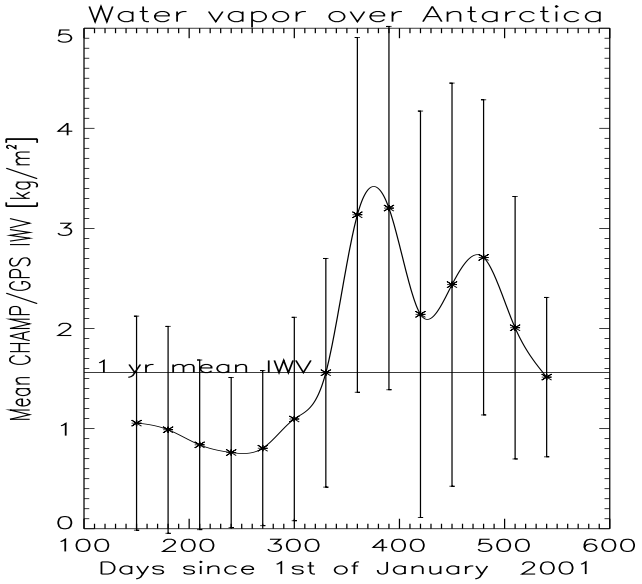

Figure 5.7: Running 60-day mean values of the vertically IWV over Antarctica derived from CHAMP/GPS water vapor data. The mean IWV over one year (between day 134 and day 499) is 1.56 ± 1.57 kg/m^2.

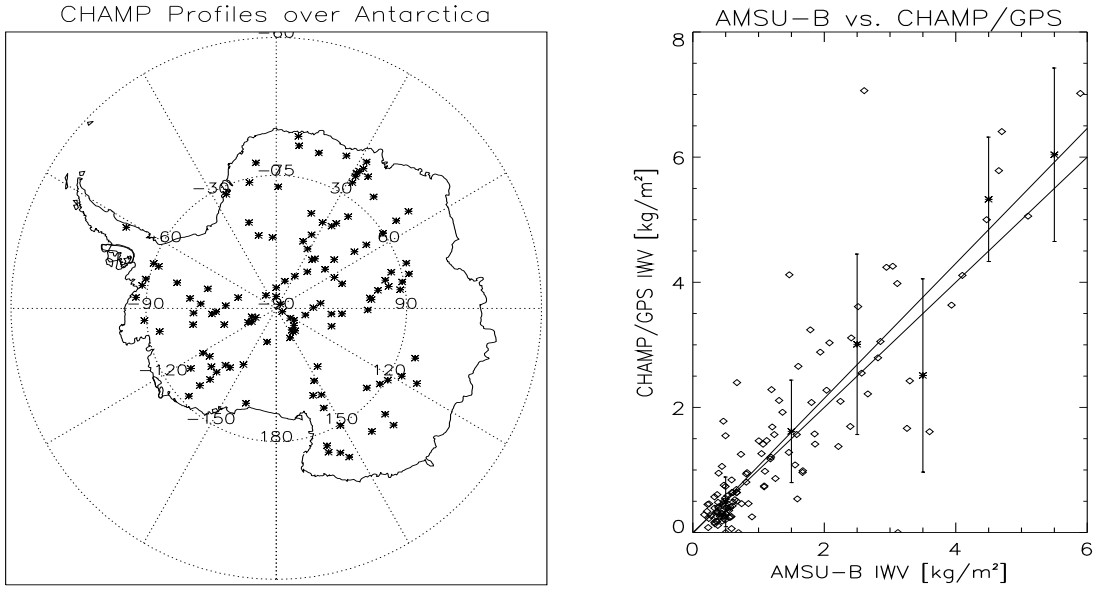

Figure 5.8: **Left:** CHAMP water vapor profiles over Antarctica between the 14th of May 2001 and the 27th of March 2002. **Right:** Comparison between the vertically IWV over Antarctica derived from AMSU-B using the algorithm of Miao et al. (2001) and from CHAMP/GPS at the positions shown in Figure 1: The error bars show the IWV mean and standard deviation of all CHAMP/GPS radio occultations for AMSU-B IWV in a range ± 0.5 kg/m^2 around the mean AMSU-B IWV. The 1:1 line as well as a linear fit are given.

using the following equation,

$$W \sec\theta = C_0 + C_1 \ln \eta_c \tag{5.2}$$

with $i, j, k \in 20, 19, 18$ for $0.0 \leq W \sec\theta \leq 1.5$ kg/m^2 and $i, j, k \in 20, 19, 17$ for $1.5 < W \sec\theta \leq 6.0$ kg/m^2. Here ΔT_{ij} is the brightness temperature difference between channels i and j of AMSU-B, W the vertically IWV, θ is the angle of observation and C_0, C_1, b_{ij} and b_{jk} are constants. For further details see Miao (1998) or Miao et al. (2001).

Figure 5.8 (left) shows the mean tangent point positions of the radio occultation profiles taken over Antarctica between the 14th of May 2001 and the 27th of March 2002 which match AMSU-B data of NOAA-15. The horizontal distance between both datasets is limited to 8 km. The time difference between the CHAMP/GPS radio occultation measurement and the NOAA-15 overpass is less than 30 minutes.

In Figure 5.8 (right) a comparison between the vertically IWV derived from CHAMP/GPS and from AMSU-B is shown. The mean difference AMSU-B/IWV − CHAMP/GPS IWV between both datasets is with -0.08 kg/m^2 quite low and the standard deviation about 0.79 kg/m^2. A linear regression between the CHAMP/GPS IWV data (G) and the AMSU-B IWV data (A) gives

$$G = -0.01 + 1.08 \times A. \tag{5.3}$$

Due to the independence of both datasets this result shows that both algorithms allow to obtain the IWV with low standard deviations over Antarctica. Therefore they should be assimilated into NWP models within the near future.

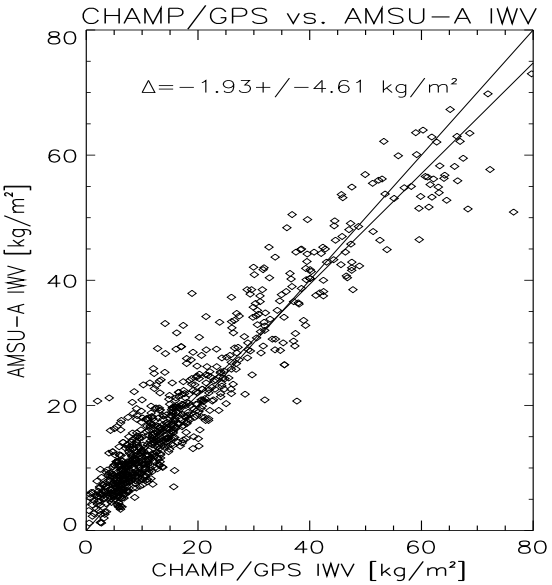

Figure 5.9: Comparison of CHAMP/GPS IWV with AMSU-A IWV over oceans worldwide. Here the NOAA/NESDIS Total Precipitable Water (TPW) algorithm is applied. Δ is the difference between CHAMP/GPS IWV and AMSU-A IWV.

Figure 5.9 shows a comparison of the IWV derived from CHAMP/GPS and from AMSU-A. Over the tropics high integrated water vapor values of up to 80 kg/m^2 will be reached. The standard deviation of the differences between CHAMP/GPS IWV and AMSU-A IWV is with 4.61 kg/m^2 larger than between the HRM and AMSU-A over the BALTEX area. AMSU-A shows also slightly (1.93 kg/m^2) larger mean values compared with CHAMP/GPS IWV. To derive the IWV from the AMSU-A data the NOAA/NESDIS algorithm is applied. For details see chapter 5.4.

Chapter 6

Conclusions

The atmospheric water vapor content is one of the most important parameters for the hydrological cycle. In order to investigate the energy and water balance over the BALTEX region, different time series of the specific humidity profiles and vertically integrated water were calculated with the hydrostatic regional weather forecast model HRM (**H**igh resolution **R**egional **M**odel) of the Deutscher Wetterdienst. To validate the HRM model different time series of the model were compared with groundbased and spaceborne GPS data within the BALTEX study region and the PIDCAP and BRIDGE periods.

High correlations (around 0.9) between the HRM IWV and GPS IWV were found. It is shown that the analysis data used to initialize the HRM model can explain a large part of the mean difference between the IWV from the model and the GPS data. The application of ECMWF analysis data has shown significant lower mean IWV differences and similar standard deviations compared with EM3AN analysis data. Comparisons between GPS data and radiosonde data have also shown similar standard deviations. GPS stations equipped with surface pressure sensors show about 0.29 kg/m^2 lower mean standard deviation compared with GPS stations with interpolated surface pressure. Different interpolation errors may explain this difference. The forecast error (i.e. the standard deviation) of the HRM model increases with time.

Specific humidities and the IWVs were determined from the refractivity profiles of the radio occultations of GPS/MET and CHAMP/GPS using an iterative algorithm of Gorbunov and Sokolovski (1993). The comparisons of the specific humidity profiles have shown that both receivers, GPS/MET and CHAMP/GPS, measure significantly lower mean specific humidities below about 4 km. This is e.g. supported by comparisons between the HRM model and the ECMWF analysis data as well as between the HRM model and radiosonde ascents at Lindenberg/Germany which have shown lower mean absolute differences of about 0.2 g/kg. The standard deviations of the difference between HRM and CHAMP/GPS are similar to the standard deviations between HRM and the radiosonde ascents. The TERRA/MODIS dataset of the 1st of December 2001 1100 UTC shows slightly larger standard deviations of up to 2 g/kg but smaller mean specific humidity differences to the HRM model by comparing 18142 profiles with similar large ranges of specific humidities like from CHAMP/GPS.

If the bias due to the multipath problem or due to noise contributions influencing the GPS phase tracking process can significantly be reduced, the CHAMP/GPS data are a valuable source of specific humidity data and should consequently be

assimilated into NWP models for Europe. The slightly larger standard deviations of TERRA/MODIS compared with the HRM could be a problem by using the TERRA/MODIS data for assimilation into NWP models which maybe solved by taking mean values before assimilation. For further details about the assimilation techniques see e.g. Kuo et al., 1993. However, due to the good coverage, the high horizontal resolution of the TERRA/MODIS data of about 5×5 km^2 and the acceptable low mean specific humidity difference between TERRA/MODIS and HRM the MOD-07 product could also supplement the radiosonde data quite well, especially in data sparse regions, and should be assimilated into NWP models.

Since the 14th of May 2001 limb sounding observations from CHAMP observing the satellites of the US Global Positioning System (GPS) are available also worldwide. Due to the sufficient accuracy of the specific humidities and of the IWVs derived from the phase delay measurements as well as the homogeneous coverage of Antarctica with radio occultations CHAMP/GPS is a valuable source of a validation of other spaceborne data also over Antarctica and other remote areas. To derive the IWV over Antarctica from the four channels 17 to 20 of AMSU-B an algorithm of Miao (1998) derived for the same frequencies of SSM/T2 is applied. The mean difference between both datasets is with -0.08 kg/m^2 quite low and the standard deviation about 0.79 kg/m^2. The annual mean IWV derived from the first year of CHAMP/GPS data over Antarctica is about 1.56 ± 1.57 kg/m^2. A similar result was obtained from Miao et al. (2001) from SSM/T2 data for the year 1997. The independence of both datasets shows that both datasets are valuable sources for the IWV over Antarctica.

Chapter 7

Publications

K.-P.Johnsen and B.Rockel: Validation of a regional weather forecast model with GPS data, Physics and Chemistry of the Earth, Vol.26, Part B, No.5−6, pages 415−419, 2001

K.-P.Johnsen and B.Rockel: Validation of the NWP model HRM with ground-based GPS data, Physics and Chemistry of the Earth, Vol.26, Part A, No.6−8, pages 463−466, 2001

K.-P.Johnsen and S.Q.Kidder: Water vapor over Europe obtained from remote sensors and compared with a hydrostatic NWP model, Physics and Chemistry of the Earth, Vol.27, No.4−5, pages 371−375, 2002

K.-P.Johnsen: NWP model specific humidities compared with CHAMP/GPS and TERRA/MODIS data, *accepted for:* Proceedings of First CHAMP Science Meeting, Geoscience Series, Springer Publishing House, 2002

K.-P.Johnsen, J.Miao and S.Q. Kidder: Comparison of atmospheric water vapor over Antarctica derived from CHAMP/GPS and AMSU-B data *submitted to:* Physics and Chemistry of the Earth, 2002

K.-P.Johnsen: GPS water vapour estimates compared with a NWP model within the BALTEX region *Proceedings of IEEE International Geoscience and Remote Sensing Symposium (IGARSS)*, Sydney, Australia, 2001

K.-P.Johnsen: Water vapour within the BALTEX region obtained from ground-based and spaceborne sensors, *in: Third Study Conference on BALTEX* (Mariehamn /Finland), Editor: J.Meywerk, International BALTEX Secretariat, Publ. No.20, GKSS Research Centre, Geesthacht, Germany, pages 99−100, 2001

K.-P.Johnsen: Comparison of a regional weather forecast model with ground-based GPS and NOAA/AMSU-A data, *in:* Proceedings of COST Action 716 (Ex-

ploitation of Ground-Based GPS for Meteorology) Workshop, 28./29.1.2002, GeoForschungsZentrum Potsdam, Germany, 2002

Bibliography

[1] M. Bevis, S. Businger, T.A. Herring, C.Rocken, R.A. Anthes, and R.H.Ware. GPS Meteorology:Remote Sensing of Atmospheric Water Vapor Using the Global Positioning System. *Journal of Geophysical Research*, 97(D14):15787–15801, 1992.

[2] G. Beyerle, M.E. Gorbunov, C. Marquardt, C. Reigber, T. Schmidt, and J. Wickert. Inverting gps radio occultation data using the canonical transform method: Results from simulation studies and champ observations. *Poster; European Geophysical Society assembly, Nice, France*, 2002.

[3] L. Cucurull, B. Navascues, G. Ruffini, P. Elosegui, A. Rius, and J. Vila. The Use of GPS to Validate NWP Systems:The HIRLAM Model. *Journal of Atmospheric and Oceanic Technology*, 17:773–787, 2000.

[4] T.R. Emardson, G. Elgered, and J.M. Johansson. Three months of continuous monitoring of atmospheric water vapor with a network of Gobal Positioning System receivers. *Journal of Geophysical Research*, 103(D2):1807–1820, 1998.

[5] T.R. Emardson, J. Johansson, and G. Elgered. The Systematic Behavior of Water Vapor Estimates Using Four Years of GPS Observations. *IEEE Transactions on Geoscience and Remote Sensing*, 38(1):324–329, 2000.

[6] G. Fjeldbo and V.R. Eshelman. The bistatic radar-occultation method for the study of planetary ionospheres. *Journal of Geophysical Research*, 70:3217–3225, 1965.

[7] G. Fjeldbo and V.R. Eshleman. The atmosphere of Mars analyzed by integral inversion of the Mariner IV occultation data. *Planet Space Sci.*, pages 1035–1059, 1968.

[8] G. Fjeldbo and A.J. Kliore. The neutral atmosphere of venus as studied with the Mariner V radio occultation experiments. *Astron. J.*, (76):123–139, 1971.

[9] G. Gendt, C. Reigber, and G. Dick. Near Real-Time Water Vapor Estimation in a German GPS Network - First Results from the Ground Program of the HGF GASP Project. *Physics and Chemistry of the Earth*, 26 Part A(6-8):413–416, 2001.

[10] M.E. Gorbunov and A.S. Gurvich. Microlab-1 experiment: Multipath effects in the lower troposphere. *Journal of Geophysical Research*, 103(D12):13819–13826, 1998.

[11] M.E. Gorbunov and S.V. Sokolovskiy. Remote sensing of refractivity from space for global observations of atmospheric parameters. Technical Report 119, Max-Planck-Institute for meteorology, Hamburg, Germany, 1993.

[12] N. Grody, F. Weng, and R. Ferraro. Application of AMSU for obtaining water vapor, cloud liquid water, precipitation, snow cover, and sea ice concentration. In *10th International TOVS Study Conference*, Boulder, Colorado, USA, 1999.

[13] G.A. Hajj, E.R. Kursinski, L.J. Romans, W.I. Bertiger, and S.S. Leroy. A technical description of atmospheric sounding by GPS occultation. *Journal of Atmospheric and Solar-Terrestrial Physics*, 64:451–469, 2002.

[14] R.F. Hanssen, T.M. Weckwerth, H.A. Zebker, and R. Klees. High-Resolution Water Vapor Mapping from Interferometric Radar Measurements. *Science*, 283:1297–1299, 1999.

[15] D.P. Hinson, F.M. Flasar, A.J. Kliore, P.J. Schinder, J.D. Twicken, and R. G. Herrera. Jupiter's ionosphere: Results from the first galileo radio occultation experiment. *Geophysical Research Letters*, (24):2107–2110, 1997.

[16] P. Hoeg and G. Kirchengast. ACE+ - Atmosphere and Climate Explorer based on GPS, GALILEO, and LEO-LEO Radio Occultation (ESA Earth Explorer Opportunity Mission Proposal). *Wissenschaftliche Berichte IGAM/University of Graz, Austria, 121 pp.*, 2002.

[17] D.A. Howarth. Seasonal variations in the verically integrated water vapor transport fields over the southern hemisphere. *Monthly Weather Review*, 111:1259–1272, 1983.

[18] S.S. Jacobs, H.H. Hellmer, C.S.M. Doake, A. Jenkins, and R.M. Frolich. Melting of ice shelves and the mass balance of Antarctica. *J. Glaciol.*, 38:619–637, 1992.

[19] K.-P. Johnsen and S.Q. Kidder. Water vapor over Europe obtained from remote sensors and compared with a hydrostatic NWP model. *Physics and Chemistry of the Earth*, 27:371–375, 2002.

[20] K.-P. Johnsen and B. Rockel. Validation of a regional weather forecast model with GPS data. *Physics and Chemistry of the Earth*, 26 Part A(5–6):415–419, 2001 a.

[21] K.-P. Johnsen and B. Rockel. Validation of the NWP Model HRM with Ground-based GPS Data. *Physics and Chemistry of the Earth*, 26 Part B(6–8):463–466, 2001 b.

[22] R.L. Jones and J.F.B. Mitchell. Is water vapour understood ? *Nature*, 353:212, 1991.

[23] A.J. Kliore, D.L. Cain, G.S. Levy, V.R. Eshleman, G. Fjeldbo, and F.D. Drake. Occultation experiment: results of the first direct measurement of mars' atmosphere and ionosphere. *Science*, 149:1243–1248, 1965.

[24] A.J. Kliore, G. Fjeldbo, B.L. Seidel, D.N. Sweetham, T.T. Sesplaukis, P.M. Woiceshyn, and S.I. Rasool. The atmosphere of io from pioneer 10 radio occultation measurements. *Icarus*, (24):407–410, 1975.

[25] A.J. Kliore and I.R. Patel. Thermal structure of the atmosphere of Venus from Pioneer Venus radio occultations. *Icarus*, 52:320–334, 1982.

[26] Y.H. Kuo, Y.-R. Guo, and E.R. Westwater. Assimilation of Precipitable Water Measurements into a Numerical Model. *Monthly Weather Review*, 121:1215–1238, 1993.

[27] Y.H. Kuo, X. Zuo, and Y.-R. Guo. Variational Assimilation of Precipitable Water Using a Nonhydrostatic Mesoscle Adjoint Model. Part I: Moisture Retrieval and Sensitivity Experiments. *Monthly Weather Review*, 124:122–147, 1996.

[28] E.R. Kursinski, D. Flittner, B. Herman, D. Feng, S. Snydergaard, and D. Ward. An Active Microwave Limb Sounder for Profiling Water Vapor, Ozone, Temperture, Geopotential of Pressure Surfaces and Clouds. *NASA's Earth System Technology Conference (ESTC)*, Pasadena, CA, June 12, 2002.

[29] E.R. Kursinski, G.A. Hajj, J.T. Schofield, R.P.Linfied, and K.R. Hardy. Observing Earth's atmosphere with radio occulation measurements using the Global Positioning System. *Journal of Geophysical Research*, 102(D19):23429–23465, 1997.

[30] G.F. Lindal. The atmosphere of Neptune: An analysis of radio occultation daata acquired with Voyager 2. *Astron. J.*, 103:967–982, 1992.

[31] G.F. Lindal, J.R. Lyons, G.L. Sweetham, and V.R. Eshleman. The atmosphere of Uranus: Results of radio occultation measurements with Voyager 2. *Geophysical Research Letters*, 14:14987–15001, 1987.

[32] G.F. Lindal, G.L. Sweetham, and V.R. Eshleman. The atmosphere of Saturn: An analysis of the Voyager radio occultation measurements. *Astron. J.*, 90:1136–1146, 1985.

[33] G.F. Lindal, G.E. Wood, H.B. Hotz, D.N. Sweetnam, V.R. Eshleman, and G.L. Tyler. The atmosphere of Titan; An analysis of the Voyager 1 radio occultation measurements. *Icarus*, 53:248–263, 1983.

[34] W.P. Menzel and L.E. Gumley. MODIS Atmospheric Profile Retrieval Algorithm Theoretical Basis Document. Technical Report Version 4, NOAA/NESDIS, University of Wisconsin-Madison, Madison, WI, 1998.

[35] J. Miao. *Retrieval of Atmospheric Water Vapor Content in Polar Regions Using Spaceborne Microwave Radiometry.* PhD thesis, Reports on Polar Research 289, Alfred Wegener Institute for Polar and Marine Research, Bremerhaven, Germany, 1998.

[36] J. Miao, K. Kunzi, G. Heygster, T.A. Lachlan-Cope, and J. Turner. Atmospheric water vapor over Antarctica derived from Special Sensor Microwave/Temperature 2 data. *Journal of Geophysical Research*, 106(D10):10187–10203, 2001.

[37] R. Ohtani and I. Naito. Comparisons of GPS-derived percipitable water vapors with radiosonde observations in Japan. *Journal of Geophysical Research*, 105(D22):26917–26929, 2000.

[38] E. Raschke. Water Vapour in the Atmosphere. Technical Report Workpackage HCP of the CM-SAF, 3001393 - RIN, Deutscher Wetterdienst, Offenbach, Germany, 2002.

[39] E. Raschke, J. Meywerk, K. Warrach, U. Andrea, S. Bergstroem, F. Beyrich, F. Bosveld, K. Bumke, C. Fortelius, L.-P. Graham, S.-E. Gryning, S. Halldin, L. Hasse, M. Heikinheimo, H.-J. Isemer, D. Jacob, I. Jauja, K.-G. Karlsson, S. Keevallik, J. Koistinen, A. van Lammeren, U. Lass, J. Launianen, A. Lehmann, B. Liljebladh, M. Lobmeyr, W. Matthaeus, T. Mengelkamp, D.B. Michelson, J. Napiorkowski, A. Omstedt, J. Piechura, B. Rockel, F. Rubel, E. Ruprecht, A.-S. Smedman, and A. Stigebrandt. The Baltic Sea Experiment (BALTEX): A European Contribution to the Investigation of the Energy and Water Cycle over a Large Drainage Basin. *Bulletin of the American Meteorological Society*, 82(11):2389–2413, 2001.

[40] W.G. Read, J.W. Waters, D.A. Flower, L. Froidevaux, R.F. Jarnot, D.L. Hartmann, R.S. Harwood, and R.B. Rood. Upper-Tropospheric Water Vapor from UARS MLS. *Bulletin of the American Meteorological Society*, 76(12):2381–2389, 1995.

[41] C. Rocken, R. Anthes, M. Exner, D. Hunt, S. Sokolovskiy, R. Ware, M. Gorbunov, W. Schreiner, D. Feng, B. Herman, Y.H. Kuo, and X. Zuo. Analysis and validation of GPS/MET data in the neutral atmosphere. *Journal of Geophysical Research*, 102(D25):29849–29866, 1997.

[42] C. Rocken, T. Van Hove, J. Johnson, F. Solheim, R.H. Ware, M. Bevis, S. Businger, and S. Chiswell. GPS/STORM - GPS sensing of atmospheric water vapor for meteorology. *Journal of Atmospheric and Oceanic Technology*, 12:468–478, 1995.

[43] C. Rocken, R. Ware, T. Van Hove, F. Solheim, C. Alber, J. Johnson, M. Bevis, and S. Businger. Sensing atmospheric water vapor with the Global Positioning System. *Geophysical Research Letters*, 20:2631–2634, 1993.

[44] W.L. Smith, H.M. Woolf, and A.J. Schriener. Simultaneous retrieval of surface and atmospheric parameters: a physical and analytically direct approach. In A. Deepak, H.E. Fleming, and M.T. Chahine, editors, *Advances in Remote Sensing*, pages 221–232, ISBN 0-937194-07-7, 1985.

[45] F.S. Solheim, J. Vivekanandan, R.H. Ware, and C. Rocken. Propagation Delays Induced in GPS Signals by Dry Air, Water Vapor, Hydrometeors and Other Particulates. *Journal of Geophysical Research*, 104:9663–9670, 1999.

[46] V.V. Vorob'ev and T.G. Krasil'nikova. Estimation of the accuracy of the atmospheric refractive index recovery from doppler shift measurements at freqencies used in the NAVSTAR system. *Physical Atmospheric and Oceanic Sciences*, (29):602–609, 1994.

[47] F. Weng, R.R. Ferraro, and N.C. Grody. Effects of cross-scan asymmetry of brightness temperatures on retrieval of atmospheric and surface parameters. In P. Pampaloni and S. Paloscia, editors, *Microwave Radiometry and Remote Sensing of the Earth and Atmosphere*, pages 255–262, Netherlands, 2000. VSP.

[48] J. Wickert. Das CHAMP-Radiookkultationsexperiment: Algorithmen, Prozesssierungssystem und erste ergebnisse. Technical Report Scientific Technical Report STR02/07, GeoForschungsZentrum, Potsdam, Germany, 2002.

[49] C. Zuffada, G.A. Hajj, and E.R. Kursinski. A novel approach to atmospheric profiling with a mountain-based or airborne GPS receiver. *Journal of Geophysical Research*, 104(D20):24435–24447, 1999.